
Deep Sketched Output Kernel Regression for Structured Prediction

Tamim El Ahmad*
LTCI, Télécom Paris
IP Paris
France
tamim.elahmad@telecom-paris.fr

Junjie Yang*
LTCI, Télécom Paris
IP Paris
France
junjie.yang@telecom-paris.fr

Pierre Laforgue
Department of Computer Science
University of Milan
Italy
pierre.laforgue@unimi.it

Florence d'Alché-Buc
LTCI, Télécom Paris
IP Paris
France
florence.dalche@telecom-paris.fr

Abstract

By leveraging the kernel trick in the output space, kernel-induced losses provide a principled way to define structured output prediction tasks for a wide variety of output modalities. In particular, they have been successfully used in the context of surrogate non-parametric regression, where the kernel trick is typically exploited in the input space as well. However, when inputs are images or texts, more expressive models such as deep neural networks seem more suited than non-parametric methods. In this work, we tackle the question of how to train neural networks to solve structured output prediction tasks, while still benefiting from the versatility and relevance of kernel-induced losses. We design a novel family of deep neural architectures, whose last layer predicts in a data-dependent finite-dimensional subspace of the infinite-dimensional output feature space deriving from the kernel-induced loss. This subspace is chosen as the span of the eigenfunctions of a randomly-approximated version of the empirical kernel covariance operator. Interestingly, this approach unlocks the use of gradient descent algorithms (and consequently of any neural architecture) for structured prediction. Experiments on synthetic tasks as well as real-world supervised graph prediction problems show the relevance of our method.

1 Introduction

Learning to predict complex outputs, such as graphs or any other composite object, raises many challenges in machine learning (Bakir et al., 2007; Nowozin and Lampert, 2011; Deshwal et al., 2019). The most important of them is undoubtedly the difficulty of leveraging the geometry of the output space. In supervised graph prediction, for instance, it is often required to use node permutation-invariant and node size-insensitive distances, such as the Fused Gromov-Wasserstein distance (Vayer et al., 2019). In that regard, surrogate methods such as Output Kernel Regression (Weston et al., 2003; Geurts et al., 2006; Kadri et al., 2013) offer a powerful and flexible framework by using the kernel trick in the output space. By appropriately choosing the output kernel, it is possible to incorporate various kinds of information, both in the model and in the loss function (Nowak et al., 2019; Ciliberto

¹Equal contribution.

et al., 2020; Cabannes et al., 2021). One important limitation of this approach, however, is that the induced output features may be infinite-dimensional.

If leveraging the kernel trick in the input space may be a solution (Cortes et al., 2005; Brouard et al., 2016b), such non-parametric methods are usually outperformed by more expressive models such as neural networks when input data consist of images or texts. In the context of structured prediction, deep learning has led to impressive results for specific tasks, such as semantic segmentation (Kirillov et al., 2023) or the protein 3D structure prediction (Jumper et al., 2021). To create versatile deep models, the main approach explored in the literature is the energy-based approach, which consists of converting structured prediction into learning a scalar score function (LeCun et al., 2006; Belanger and McCallum, 2016; Gygli et al., 2017; Lee et al., 2022). However, these methods usually fail to go beyond structured prediction problems which can be reformulated as high-dimensional multi-label classification problems, as pointed out by Graber et al. (2018). Besides, this approach requires a two-step strategy, since the energy function is first learned thanks to the training data, and then maximized at inference time. To obtain an end-to-end model, Belanger et al. (2017) uses direct risk minimization techniques, and Tu and Gimpel (2018) introduces inference networks, a neural architecture that approximates the inference problem. In this work, we choose to benefit from the versatility of kernel-induced losses, and deploy it to neural networks. To this end, we address the infinite-dimensionality of the output features by computing a finite-dimensional basis within the output feature space, defined as the eigenbasis of a sketched version of the output empirical covariance operator.

Sketching (Mahoney et al., 2011; Woodruff, 2014) is a dimension-reduction technique based on random linear projections. In the context of kernel methods, it has mainly been explored through the so-called Nyström approximation (Williams and Seeger, 2001; Rudi et al., 2015), or via specific distributions such as Gaussian or Randomized Orthogonal Systems (Yang et al., 2017; Lacotte and Pilanci, 2022). Previous works tackle sketched scalar kernel regression by providing a low-rank approximation of the Gram matrix (Drineas et al., 2005; Bach, 2013), reducing the number of parameters to learn at the optimization stage (Yang et al., 2017; Lacotte and Pilanci, 2022), providing data-dependent random features (Williams and Seeger, 2001; Yang et al., 2012; Kpotufe and Sriperumbudur, 2020), or leveraging an orthogonal projection operator in the feature space (Rudi et al., 2015). This last interpretation has been used to learn large-scale dynamical systems (Meanti et al., 2023), and structured prediction (El Ahmad et al., 2024).

In our proposition to solve structured prediction from complex input data, we make the following contributions:

- We introduce Deep Sketched Output Kernel Regression, a novel family of deep neural architectures whose last layer predicts a data-dependent finite-dimensional representation of the outputs, that lies in the infinite-dimensional feature space deriving from the kernel-induced loss.
- This last layer is computed beforehand, and is the eigenbasis of the sketched empirical covariance operator, unlocking the use of gradient-based techniques to learn the weights of the previous layers for any neural architecture.
- We empirically show the relevance of our approach on a synthetic least squares regression problem, and provide a strategy to select the sketching size.
- We show that DSOKR performs well on two text-to-molecule datasets.

2 Deep Sketched Output Kernel Regression

In this section, we set up the problem of structured prediction. Specifically, we consider surrogate regression approaches for kernel-induced losses. By introducing a last layer able to make predictions in a Reproducing Kernel Hilbert Space (RKHS), we unlock the use of deep neural networks as hypothesis space.

Consider the general regression task from an input domain \mathcal{X} to a structured output domain \mathcal{Y} (e.g., the set of labeled graphs of arbitrary size). Learning a mapping from \mathcal{X} to \mathcal{Y} naturally requires taking into account the structure of the output space. One way to do so is the *Output Kernel Regression*

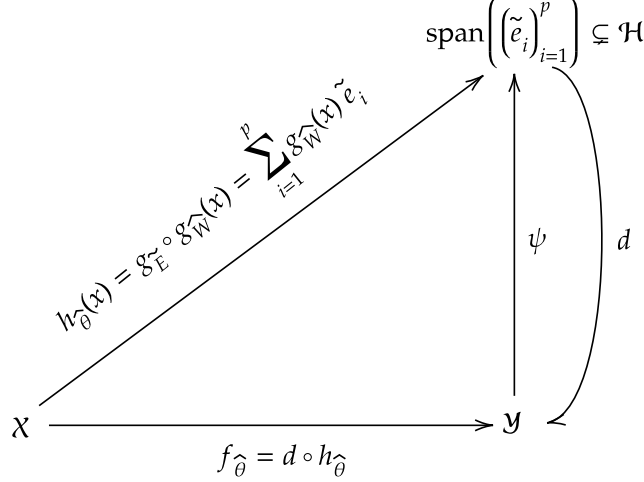


Figure 1: Illustration of DSOKR model.

(OKR) framework (Weston et al., 2003; Cortes et al., 2005; Geurts et al., 2006; Brouard et al., 2011, 2016b), which is part of the family of surrogate regression methods (Ciliberto et al., 2016, 2020).

Output Kernel Regression. A positive definite (p.d.) kernel $k : \mathcal{Y} \times \mathcal{Y} \rightarrow \mathbb{R}$ is a symmetric function such that for all $n \geq 1$, and any $(y_i)_{i=1}^n \in \mathcal{Y}^n$, $(\alpha_i)_{i=1}^n \in \mathbb{R}^n$, we have $\sum_{i,j=1}^n \alpha_i k(y_i, y_j) \alpha_j \geq 0$. Such a kernel is associated with a canonical feature map $\psi : y \in \mathcal{Y} \mapsto k(\cdot, y)$, which is uniquely associated with a Hilbert space of functions $\mathcal{H} \subset \mathbb{R}^{\mathcal{Y}}$, the RKHS, such that $\psi(y) \in \mathcal{H}$ for all $y \in \mathcal{Y}$, and $h(y) = \langle h, \psi(y) \rangle_{\mathcal{H}}$ for any $(h, y) \in \mathcal{H} \times \mathcal{Y}$. Given a p.d. kernel k , ψ its canonical feature map and \mathcal{H} its RKHS, the OKR approach that we consider in this work exploits the kernel-induced squared loss:

$$\Delta(y, y') := \|\psi(y) - \psi(y')\|_{\mathcal{H}}^2 = k(y, y) - 2k(y, y') + k(y', y'). \quad (1)$$

The versatility of loss (1) stems from the large variety of kernels that have been designed to compare structured objects (Gärtner, 2008; Korba et al., 2018; Borgwardt et al., 2020). In multi-label classification, for instance, choosing the linear kernel or the Tanimoto kernel induces respectively the Hamming and the F1-loss (Tanimoto, 1958). In label ranking, Kemeny and Hamming embeddings define Kendall’s τ distance and the Hamming loss (Korba et al., 2018; Nowak et al., 2020) respectively. For sequence prediction tasks, n-gram kernels have been proven useful (Cortes et al., 2007; Kadri et al., 2013; Nowak et al., 2020), while an abundant collection of kernels has been designed for graphs, based either on bags of structures or information propagation, see Appendix B and Borgwardt et al. (2020) for examples.

If kernel-induced losses can be computed easily thanks to the kernel trick, note that most of them are however non-differentiable. In particular, this largely compromises their use within deep neural architectures, that are however key to achieve state-of-the-art performances in many applications. In this work, we close this gap and propose an approach that benefits from both the expressivity of neural networks for input image/textual data, as well as the relevance of kernel-induced losses for structured outputs. Formally, let ρ be a joint probability distribution on $\mathcal{X} \times \mathcal{Y}$. Our goal is to design a family $(f_{\theta})_{\theta \in \Theta} \subset \mathcal{Y}^{\mathcal{X}}$ of neural networks with outputs in \mathcal{Y} that can minimize the kernel-induced loss, i.e., that can solve

$$\min_{\theta \in \Theta} \mathbb{E}_{(x,y) \sim \rho} \left[\|\psi(y) - \psi(f_{\theta}(x))\|_{\mathcal{H}}^2 \right]. \quad (2)$$

To do so, we assume that we can access a training sample $\{(x_1, y_1), \dots, (x_n, y_n)\}$ drawn i.i.d. from ρ . Since learning f_{θ} through ψ is difficult, we employ a two-step method. First, we solve the surrogate empirical problem

$$\hat{\theta} \in \arg \min_{\theta \in \Theta} L(\theta) = \arg \min_{\theta \in \Theta} \frac{1}{n} \sum_{i=1}^n \|h_{\theta}(x_i) - \psi(y_i)\|_{\mathcal{H}}^2, \quad (3)$$

where $(h_\theta)_{\theta \in \Theta} \subset \mathcal{H}^{\mathcal{X}}$ is a family of neural networks with outputs in \mathcal{H} . We then retrieve the solution by solving for any prediction the pre-image problem

$$f_{\hat{\theta}}(x) = \arg \min_{y \in \mathcal{Y}} \|h_{\hat{\theta}}(x) - \psi(y)\|_{\mathcal{H}}^2. \quad (4)$$

This approach nonetheless raises a major challenge. Indeed, the dimension of the canonical feature space \mathcal{H} may be infinite, making the training very difficult. The question we have to answer now is: *how can we design a neural architecture that is able to learn infinite-dimensional output kernel features?*

Neural networks with infinite-dimensional outputs. We propose a novel architecture of neural networks to compute the function h_θ with values in \mathcal{H} . Let $p \geq 1$, our architecture is the composition of two networks: an input neural network, denoted $g_W : \mathcal{X} \rightarrow \mathbb{R}^p$, with generic weights $W \in \mathcal{W}$, and a last layer composed of a unique *functional* neuron, denoted $g_E : \mathbb{R}^p \rightarrow \mathcal{H}$, that predicts in \mathcal{H} . The latter depends on the kernel k used in the loss definition, and on a finite basis $E = ((e_j)_{j=1}^p) \in \mathcal{H}^p$ of elements in \mathcal{H} . We let $\theta = (W, E)$, and for any $x \in \mathcal{X}$, we have

$$h_\theta(x) := g_E \circ g_W(x), \quad (5)$$

where g_W typically implements a $L - 1$ neural architecture encompassing, multilayered perceptrons, convolutional neural networks, or transformers. Instead, g_E computes a linear combination of some basis functions $E = (e_j)_{j=1}^p \in \mathcal{H}^p$

$$g_E : z \in \mathbb{R}^p \mapsto \sum_{j=1}^p z_j e_j \in \mathcal{H}. \quad (6)$$

With this architecture, computations remain finite, and the input neural network outputs the coefficients of the basis expansion, generating predictions in \mathcal{H} .

Remark 1 (Input Neural net’s last layers). Since the neural network g_W learns the coordinates of the surrogate estimator in the basis, its last layers are always mere fully connected ones, regardless of the nature of the output data at hand.

2.1 Learning neural networks with infinite-dimensional outputs

Learning the surrogate regression model h_θ now boils down to computing $\theta = (W, E)$. We propose to solve this problem in two steps. First, we learn a suitable E using only the output training data $(\psi(y_i))_{i=1}^n$ in an unsupervised fashion. Then, we use standard gradient-based algorithms to learn W through the frozen last layer, minimizing the loss on the whole supervised training sample $(x_i, \psi(y_i))_{i=1}^n$.

Estimating the functional last unit g_E . A very first idea is to choose E as the non-orthogonal dictionary $\psi(y_j)_{j=1}^n$. But this choice induces a very large output dimension (namely, $p = n$) for large training datasets.

An alternative consists in using Kernel Principal Component Analysis (KPCA) (Schölkopf et al., 1997). Given a marginal probability distribution over \mathcal{Y} , let $C = \mathbb{E}_y[\psi(y) \otimes \psi(y)]$ be the covariance operator associated with k , and $\hat{C} = (1/n) \sum_{i=1}^n \psi(y_i) \otimes \psi(y_i)$ its empirical counterpart. Let S be the sampling operator that transforms a function $f \in \mathcal{H}$ into the vector $(1/\sqrt{n})(f(x_1), \dots, f(x_n))^\top$ in \mathbb{R}^n , and denote by $S^\#$ its adjoint. We have $S^\# : \alpha \in \mathbb{R}^n \mapsto (1/\sqrt{n}) \sum_{i=1}^n \alpha_i \psi(y_i) \in \mathcal{H}$, and $\hat{C} = S^\# S$. KPCA provides the eigenbasis of \hat{C} by computing the SVD of the output Gram matrix, for a prohibitive computational cost of $\mathcal{O}(n^3)$. In practice, though, it is often the case that the so-called *capacity condition* holds (Ciliberto et al., 2020; El Ahmad et al., 2024), i.e., that the spectrum of the empirical covariance operator enjoys a large eigendecay. It is then possible to efficiently approximate the eigenbasis of \hat{C} using random projections techniques (Mahoney et al., 2011), also known as sketching, solving this way the computational and memory issues.

Sketching for kernel methods. Sketching (Woodruff, 2014) is a dimension reduction technique based on random linear projections. Since the goal is to reduce the dependency on the number of training samples n in kernel methods, such linear projections can be encoded by a randomly drawn

matrix $R \in \mathbb{R}^{m \times n}$, where $m \ll n$. Standard examples include Nyström approximation (Meanti et al., 2020), where each row of R is randomly drawn from the rows of the identity matrix I_n , also called sub-sampling sketches, and Gaussian sketches (Yang et al., 2017), where all entries of R are i.i.d. Gaussian random variables. As they act as a random training data sub-sampler and then largely reduce both the time and space complexities induced by kernel methods, sub-sampling sketches are the most popular sketching type applied to kernels, while Gaussian sketches are less computationally efficient but offer better statistical properties. Hence, given a sketching matrix $R \in \mathbb{R}^{m \times n}$, one can define $\tilde{\mathcal{H}}_{\mathcal{Y}} = \text{span}((\sum_{j=1}^n R_{ij} \psi(y_j))_{i=1}^m)$ which is a low-dimensional linear subspace of \mathcal{H} of dimension at most m . One can even compute the basis \tilde{E} of $\tilde{\mathcal{H}}_{\mathcal{Y}}$, providing the last layer $g_{\tilde{E}}$.

Sketching to estimate g_E . We here show how to compute the basis \tilde{E} of $\tilde{\mathcal{H}}_{\mathcal{Y}}$. Let $m < n$, and $R \in \mathbb{R}^{m \times n}$ be a sketching matrix. Let $\tilde{K} = RKR^T \in \mathbb{R}^{m \times m}$ be the sketched Gram matrix, and $\{(\sigma_i(\tilde{K}), \tilde{v}_i), i \in [m]\}$ its eigenpairs, in descending order. We set $p = \text{rank}(\tilde{K})$. Note that $p \leq m$, and that $p = m$ for classical examples, e.g. full-rank K and sub-sample without replacement or Gaussian R . The following proposition provides the eigenfunctions of the sketched empirical covariance operator.

Proposition 1. (El Ahmad et al., 2024, Proposition 2) *The eigenfunctions of the sketched empirical covariance operator $\tilde{C} = S^\# R^T R S$ are the $\tilde{e}_j = \sqrt{\frac{n}{\sigma_j(\tilde{K})}} S^\# R^T \tilde{v}_j \in \mathcal{H}$, for $j \leq p$.*

Hence, computing the eigenfunctions of \tilde{C} provides a basis of \mathcal{H} of dimension p . Note that in sketched KPCA, which has been explored via Nyström approximation in Sterge et al. (2020); Sterge and Sriperumbudur (2022), one solves for $i = 1, \dots, m$

$$f_i = \arg \max_{f \in \mathcal{H}} \left\{ \langle f, \tilde{C} f \rangle_{\mathcal{H}} : f \in \tilde{\mathcal{H}}_{\mathcal{Y}}, \|f\|_{\mathcal{H}} = 1, f \perp \{f_1, \dots, f_{i-1}\} \right\} \quad (7)$$

where $\tilde{\mathcal{H}}_{\mathcal{Y}} = \text{span}((\sum_{j=1}^n R_{ij} \psi(y_j))_{i=1}^m)$. Let \tilde{P} be the orthogonal projector onto the basis $(\tilde{e}_1, \dots, \tilde{e}_p)$, solving Equation (7) is equivalent to compute the eigenfunctions of the projected empirical covariance operator $\tilde{P} \tilde{C} \tilde{P}$, i.e., to compute the KPCA of the projected kernel $\langle \tilde{P} \psi(\cdot), \tilde{P} \psi(\cdot) \rangle_{\mathcal{H}}$. Besides, as for the SVD of \tilde{C} , sketched KPCA needs the SVD of \tilde{K} to obtain its square root, but also requires the additional $\tilde{K}^{1/2} R K^2 R^T \tilde{K}^{1/2}$ SVD computation.

Remark 2 (Random Fourier Features). Another popular kernel approximation is the Random Fourier Features (Rahimi and Recht, 2007; Rudi and Rosasco, 2017; Li et al., 2021). They approximate a kernel function as the inner product of small random features using Monte-Carlo sampling when the kernel writes as the Fourier transform of a probability distribution. Such an approach, however, defines a new randomly approximated kernel, then a new randomly approximated loss, which can induce learning difficulties due to the bias and variance inherent to the approximation. Unlike RFF, sketching is not limited to kernels writing as the Fourier transform of a probability distribution and to defining an approximated loss, it allows the building of a low-dimensional basis within the original feature space of interest.

Learning the input neural network g_W . Equipped with the basis $\tilde{E} = (\tilde{e}_j)_{j \leq p}$, we can compute a novel expression of the loss $L(\theta) = L(\tilde{E}, W)$, see Appendix A for the proof.

Proposition 2. *Given the pre-trained basis $\tilde{E} = (\tilde{e}_j)_{j \leq p}$, $L(\tilde{E}, W)$ expresses as*

$$L(\tilde{E}, W) = \frac{1}{n} \sum_{i=1}^n \left\| g_W(x_i) - \tilde{\psi}(y_i) \right\|_2^2, \quad (8)$$

where $\tilde{\psi}(y) = (\tilde{e}_1(y), \dots, \tilde{e}_p(y))^T = \tilde{D}_p^{-1/2} \tilde{V}_p^T R k^y \in \mathbb{R}^p$, $\tilde{V}_p = (\tilde{v}_1, \dots, \tilde{v}_p)$, $\tilde{D}_p = \text{diag}(\sigma_1(\tilde{K}), \dots, \sigma_p(\tilde{K}))$, and $k^y = (k(y, y_1), \dots, k(y, y_n))$.

Finally, given \tilde{E} and Prop. 2, learning the full network h_θ boils down to learning the input neural network g_W and thus finding a solution \hat{W} to

$$\min_{W \in \mathcal{W}} \frac{1}{n} \sum_{i=1}^n \left\| g_W(x_i) - \tilde{\psi}(y_i) \right\|_2^2. \quad (9)$$

Algorithm 1 Deep Sketched Output Kernel Regression (DSOKR)

input : training $\{(x_i, y_i)\}_{i=1}^n$, validation $\{(x_i^{\text{val}}, y_i^{\text{val}})\}_{i=1}^{n_{\text{val}}}$ pairs, test inputs $\{x_i^{\text{te}}\}_{i=1}^{n_{\text{te}}}$, candidate outputs test inputs $\{y_i^c\}_{i=1}^{n_c}$, normalized output kernel k , sketching matrix $R \in \mathbb{R}^{m \times n}$, neural network g_W

init : $\tilde{K} = R K R^\top \in \mathbb{R}^{m \times m}$ where $K = (k(y_i, y_j))_{1 \leq i, j \leq n} \in \mathbb{R}^{n \times n}$

// 1. a. Training of g_E : computations for the basis \tilde{E}

- Construct $\tilde{D}_p \in \mathbb{R}^{p \times p}$, $\tilde{V}_p \in \mathbb{R}^{m \times p}$ such that $\tilde{V}_p \tilde{D}_p \tilde{V}_p^\top = \tilde{K}$ (SVD of \tilde{K})
- $\tilde{\Omega} = \tilde{D}_p^{-1/2} \tilde{V}_p^\top \in \mathbb{R}^{p \times m}$

// 1. b. Training of g_W : solving the surrogate problem

- $\tilde{\psi}(y_i) = \tilde{\Omega} R k^{y_i} \in \mathbb{R}^p, \forall 1 \leq i \leq n, \tilde{\psi}(y_i^{\text{val}}) = \tilde{\Omega} R k^{y_i^{\text{val}}} \in \mathbb{R}^p, \forall 1 \leq i \leq n_{\text{val}}$
- $\tilde{W} = \arg \min_{W \in \mathcal{W}} \frac{1}{n} \sum_{i=1}^n \left\| g_W(x_i) - \tilde{\psi}(y_i) \right\|_2^2$ (training of g_W with training $\{(x_i, \tilde{\psi}(y_i))\}_{i=1}^n$ and validation $\{(x_i^{\text{val}}, \tilde{\psi}(y_i^{\text{val}}))\}_{i=1}^{n_{\text{val}}}$ pairs and Mean Squared Error loss)

// 2. Inference

- $\tilde{\psi}(y_i^c) = \tilde{\Omega} R k^{y_i^c} \in \mathbb{R}^p, \forall 1 \leq i \leq n_c$
- $f_{\hat{\theta}}(x_i^{\text{te}}) = y_j^c$ where $j = \arg \max_{1 \leq j \leq n_c} g_{\tilde{W}}(x_i^{\text{te}})^\top \tilde{\psi}(y_j^c), \forall 1 \leq i \leq n_{\text{te}}$

return $f_{\hat{\theta}}(x_i^{\text{te}}), \forall 1 \leq i \leq n_{\text{te}}$

A classical stochastic gradient descent algorithm can then be applied to learn W . Compared to the initial loss (3), the relevance of (9) is governed by the quality of the approximation of \hat{C} by \tilde{C} . If our approach regularises the solution (the range of the surrogate estimator h_θ is restricted from \mathcal{H} to E), this restriction may not be limiting if we set $m \geq p$ high enough to capture all the information contained in \tilde{C} . We discuss strategies to correctly set m at the beginning of Section 3.

Remark 3 (Beyond the square loss). Equipped with such an architecture $g_W \circ g_E$, one can easily consider any loss that writes $\Delta(y, y') = c(\|\psi(y) - \psi(y')\|_{\mathcal{H}}^2)$, where $c : \mathbb{R}_+ \rightarrow \mathbb{R}_+$ is a non-decreasing sub-differentiable function. For instance, in the presence of output outliers, one could typically consider robust losses such as the Huber or ϵ -insensitive losses, that correspond to different choices of function c (Laforgue et al., 2020; Huber, 1964; Steinwart and Christmann, 2008).

2.2 The pre-image problem at inference time

We focus now on the decoding part, i.e., on computing

$$d \circ h_{\hat{\theta}}(x) = \arg \min_{y \in \mathcal{Y}} k(y, x) - 2g_{\tilde{W}}(x)^\top \tilde{\psi}(y) = \arg \max_{y \in \mathcal{Y}} g_{\tilde{W}}(x)^\top \tilde{\psi}(y)$$

if we assume k to be normalized, i.e. $k(y, y') = 1, \forall y, y' \in \mathcal{Y}$. For a test set $X^{\text{te}} = (x_1^{\text{te}}, \dots, x_{n_{\text{te}}}^{\text{te}}) \in \mathcal{X}^{n_{\text{te}}}$ and a candidate set $Y^c = (y_1^c, \dots, y_{n_c}^c) \in \mathcal{Y}^{n_c}$, for all $1 \leq i \leq n_{\text{te}}$, the prediction is given by

$$f_{\hat{\theta}}(x_i^{\text{te}}) = y_j^c \quad \text{where} \quad j = \arg \max_{1 \leq j \leq n_c} g_{\tilde{W}}(x_i^{\text{te}})^\top \tilde{\psi}(y_j^c). \quad (10)$$

Hence, the decoding is particularly suited to problems for which we have some knowledge of the possible outcomes, such as molecular identification problems (Brouard et al., 2016a). When the output kernel is differentiable, it may also be solved using standard gradient-based methods. Finally, some ad-hoc ways to solve the pre-image problem exist for specific kernels, see e.g., Cortes et al. (2007) for the sequence prediction via n-gram kernels, or Korba et al. (2018) for label ranking via Kemeny, Hamming, or Lehmer embeddings. The DSOKR framework is summarized in Algorithm 1.

3 Experiments

In this section, we first present a range of strategies to select the sketching size and an analysis of our proposed DSOKR on a synthetic dataset. Besides, we show the effectiveness of DSOKR through its

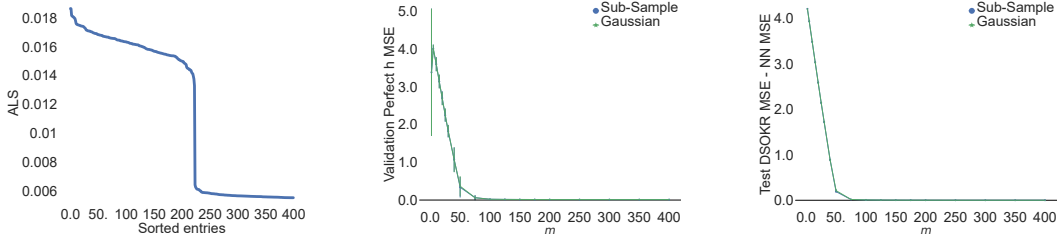


Figure 2: Sorted 400 highest ALS (left), validation MSE of *Perfect h* w.r.t. m (center) and the difference between test MSE of DSOKR and NN w.r.t. m (right).

application to two real-world Supervised Graph Prediction (SGP) tasks: SMILES to Molecule and Text to Molecule. The code to reproduce our results is available at: <https://github.com/tamim-el/dsokr>.

Sketching size selection strategy. A critical hyper-parameter of DSOKR is the sketching size m . Indeed, the optimal choice is the dimension of the subspace containing the output features. However, to estimate this dimension, one has to compute the eigenvalues of K , which has the prohibitive complexity of $\mathcal{O}(n^3)$. Hence, a first solution is to compute the Approximate Leverage Scores (ALS) as described in Alaoui and Mahoney (2015). This is an approximation of the eigenvalues of K that relies on sub-sampling $n_S < n$ entries within the whole training set. Moreover, we use another technique that we call *Perfect h*. Considering any pair (x, y) in a validation set, we replace $g_W(x)$ by the “perfect” coefficients of the expansion, i.e., for each $j = 1, \dots, p$, $\langle \tilde{e}_j, \psi(y) \rangle_{\mathcal{H}}$ and define “perfect” surrogate estimator h_{ψ} as follows

$$h_{\psi}(x) = \sum_{j=1}^p \langle \tilde{e}_j, \psi(y) \rangle_{\mathcal{H}} \tilde{e}_j = \sum_{j=1}^p \tilde{\psi}(y)_j \tilde{e}_j. \quad (11)$$

Then, we evaluate the performance of this “perfect” surrogate estimator h_{ψ} on a validation set to select m . Hence, *Perfect h* allows to select the minimal m in the range given by ALS such that the performance of h_{ψ} reaches an optimal value.

3.1 Analysis of DSOKR on Synthetic Least Squares Regression

Dataset. We generate a synthetic dataset of least-squares regression, using then a linear output kernel, with $n = 50,000$ training data points, $\mathcal{X} = \mathbb{R}^{2,000}$, $\mathcal{Y} = \mathbb{R}^{1,000}$, and $\mathcal{H} = \mathcal{Y} = \mathbb{R}^{1,000}$. The goal is to build this dataset such that the outputs lie in a subspace of \mathcal{Y} of dimension $d = 50 < 1,000$. Hence, given d randomly drawn orthonormal vectors $(u_j)_{j=1}^d$, for all $1 \leq i \leq n$, the outputs are such that $y_i = \sum_{j=1}^d \alpha(x_i)_j u_j + \varepsilon_i$, where α is a function of the inputs and $\varepsilon_i \sim \mathcal{N}(0, \sigma^2 I_{1,000})$ are i.i.d. with $\sigma^2 = 0.01$. We generate i.i.d. normal distributed inputs $x_i \sim \mathcal{N}(0, C)$, where $(\sigma_j(C) = j^{-1/2})_{j=1}^{2,000}$ and its eigenvectors are randomly drawn. Finally, we draw $H \in \mathbb{R}^{d \times 2,000}$ with i.i.d. coefficients from the standard normal distribution, and the outputs are given for $1 \leq i \leq n$ by

$$y_i = U H x_i + \varepsilon_i, \quad (12)$$

where $U = (u_1, \dots, u_d) \in \mathbb{R}^{1,000 \times d}$. We generate validation and test sets of $n_{\text{val}} = 5,000$ and $n_{\text{te}} = 10,000$ points in the same way.

Experimental settings. We first compute the ALS as described above. We take as regularisation penalty $\lambda = 10^{-4}$, sampling parameter $n_S = \sqrt{n}$ and probability vector $(p_i = 1/n)_{i=1}^n$ (uniform sampling). Then, we perform the sketching size selection strategy *Perfect h*. Note that using a linear output kernel, $\psi : y \in \mathbb{R}^{1,000} \mapsto y$, then $\tilde{e}_i = (1/\sqrt{\sigma_i(\tilde{K})}) \tilde{v}_i^{\top} R Y$, where $Y = (y_1, \dots, y_n)^{\top} \in \mathbb{R}^{n \times 1,000}$, and

$$h_{\hat{\theta}}(x) = Y^{\top} R^{\top} \tilde{V}_p \tilde{D}_p^{-1/2} g_{\tilde{W}}(x). \quad (13)$$

Finally, we perform our DSOKR model whose neural network g_W is a Single-Layer Perceptron, i.e. with no hidden layer, and compare it with an SLP whose output size is 1,000, and trained with

a Mean Squared Error loss, that we call “NN”. We select the optimal number of epochs thanks to the validation set and evaluate the performance via the MSE. We use the ADAM (Kingma and Ba, 2015) optimizer. For the *Perfect h* and DSOKR models and any sketching size $m \in [2, 400]$, we average the results over five replicates of the models. We use uniform sub-sampling without replacement and Gaussian sketching distributions.

Experimental results. Figure 2 (left) presents the sorted 400 highest leverage scores. This gives a rough estimate of the optimal sketching size since the leverage scores converge to a minimal value starting from 200 approximately, which is an upper bound of the true basis dimension $d = 50$. Figure 2 (center) shows that *Perfect h* is a relevant strategy to fine-tune m since the obtained optimal value is $m = 75$, which is very close to $d = 50$. This small difference comes from the added noise ε_i . Moreover, this value corresponds to the optimal value based on the DSOKR test MSE. In fact, Figure 2 (right) presents the performance DSOKR for many m values compared with NN. DSOKR performance converges to the NN’s performance for $m = 75$ as well. Hence, we show that DSOKR attains optimal performance if its sketching size is set as the dimension of the output marginal distribution’s range, which can be estimated thanks to the ALS and the *Perfect h* strategies. There is no difference between sub-sample and Gaussian sketching since the dataset is rather simple. Moreover, note that the neural network of the DSOKR model for $m = 75$ contains 150,075 parameters, whereas the NN model contains 2,001,000 parameters. Then, our sketched basis strategy, even in the context of multi-output regression, allows to reduce the size of the last layer, simplifying the regression problem and reducing the number of weights to learn.

3.2 SMILES to Molecule: SMI2Mol

Dataset. We use the QM9 molecule dataset (Ruddigkeit et al., 2012; Ramakrishnan et al., 2014), containing around 130,000 small organic molecules. These molecules have been processed using RDKit¹, with aromatic rings converted to their Kekule form and hydrogen atoms removed. We also remove molecules containing only one atom. Each molecule contains up to 9 atoms of Carbon, Nitrogen, Oxygen, or Fluorine, along with three types of bonds: single, double, and triple. As input features, we use the Simplified Molecular Input Line-Entry System (SMILES), which are strings describing their chemical structure. We refer to the resulting dataset as **SMI2Mol**.

Experimental set-up. Using all SMILES-Molecule pairs, we build five splits using different seeds. Each split has 131,382 training samples, 500 validation samples, and 2,000 test samples. In DSOKR, g_W is a Transformer (Vaswani et al., 2017). The SMILES strings are tokenized into character sequences as inputs for the Transformer encoder. To define the loss on output molecules, we cross-validate several graph kernels, including the Weisfeiler-Lehman subtree kernel (WL-VH) (Shervashidze et al., 2011), the neighborhood subgraph pairwise distance kernel (NSPD) (Costa and Grave, 2010), and the core Weisfeiler-Lehman subtree kernel (CORE-WL) (Nikolentzos et al., 2018). We use the implementation of the graph kernels provided by the Python library GraKel (Siglidis et al., 2020). We employ SubSample sketching for the output kernel. The sketching size m is fixed using our proposed *Perfect h* strategy. Our method is benchmarked against SISOKR (El Ahmad et al., 2024), NNbary-FGW (Brogat-Motte et al., 2022), and ILE-FGW (Brogat-Motte et al., 2022). For ILE-FGW and SISOKR, we additionally use SubSample sketching (Rudi et al., 2015) for input kernel approximation. To ensure a fair comparison, both SISOKR and ILE-FGW adopt the 3-gram kernel for the input strings, whereas NNbary-FGW and DSOKR use a Transformer encoder. The performance is evaluated using Graph Edit Distance (GED), implemented by the NetworkX package (Hagberg et al., 2008).

Experimental results. Figure 3 displays the GED obtained by *Perfect h* concerning various graph kernels. Based on this visualization, we have set the sketching sizes of WL-VH, CORE-WL, and NSPD to 3200, 3200, and 6400 respectively. Table 1 showcases the performance of various methods of SGP. Notably, DSOKR outperforms all baseline methods. It is evident that while graph kernels and the fused Gromov-Wasserstein (FGW) distance induce a meaningful feature space, the capabilities of SISOKR and ILE-FGW are constrained by the input kernels, thus highlighting the relevance of our proposed method. For further insight, a comparison of some prediction examples is provided in Figure 4 and Appendix C.1.

¹RDKit: Open-source cheminformatics. <https://www.rdkit.org>

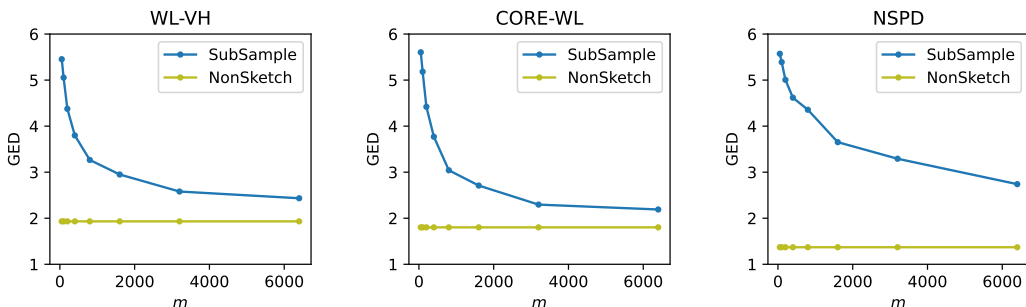


Figure 3: The GED w/ edge feature w.r.t. the sketching size m for *Perfect* h for three graph kernels on SMI2Mol ($m > 6400$ is too costly computationally).

Table 1: Edit distance of different methods on SMI2Mol test set

| | GED w/o edge feature ↓ | GED w/ edge feature ↓ |
|------------------|-------------------------------------|-------------------------------------|
| SISOKR | 3.330 ± 0.080 | 4.192 ± 0.109 |
| NNBary-FGW | 5.115 ± 0.129 | - |
| Sketched ILE-FGW | 2.998 ± 0.253 | - |
| DSOKR | 1.951 ± 0.074 | 2.960 ± 0.079 |

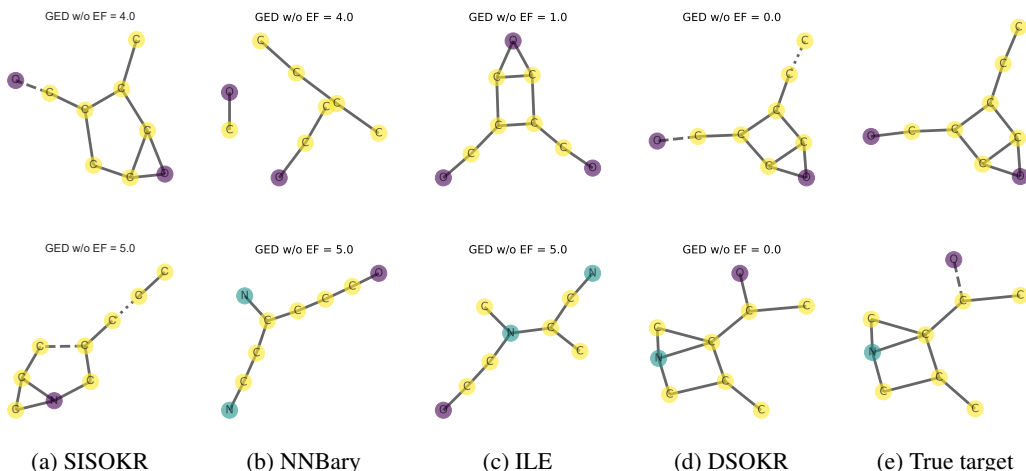


Figure 4: Predicted molecules on the SMI2Mol dataset.

3.3 Text to Molecule: ChEBI-20

Dataset. The ChEBI-20 (Edwards et al., 2021) dataset contains 33,010 pairs of compounds and descriptions. The compounds come from PubChem (Kim et al., 2016, 2019), and their descriptions (more than 20 words) from the Chemical Entities of Biological Interest (ChEBI) database (Hastings et al., 2016). The dataset is divided as follows: 80% for training, 10% for validation, and 10% for testing. The candidate set contains all compounds. The mean and median number of atoms per molecule is 32 and 25 respectively, and the mean and median number of words per description is 55 and 51 respectively.

Experimental set-up. For our method DSOKR, we use SciBERT (Beltagy et al., 2019) with an additional linear layer to parameterize g_W . The maximum length of the input tokens is set to 256. Mol2vec (Jaeger et al., 2018) is used as the output molecule representation, which is a vector of dimension 300. Based on the Mol2vec representation, we conduct cross-validation using the following

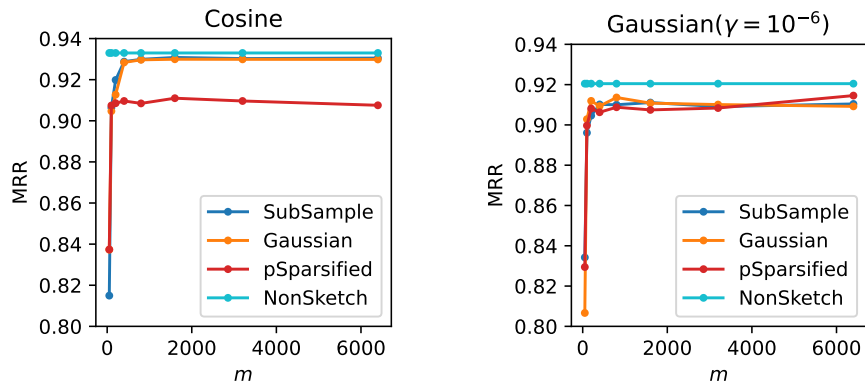


Figure 5: The MRR scores on ChEBI-20 validation set w.r.t. m for *Perfect h* when the output kernel is Cosine or Gaussian on the ChEBI-20 dataset.

Table 2: Performance of different methods on ChEBI-20 test set. All the methods based on NNs use SciBERT as input text encoder for fair comparison. The number in the ensemble setting indicates the number of single models used.

| | Hits@1 \uparrow | Hits@10 \uparrow | MRR \uparrow |
|---------------------------------------------------------------|-------------------|--------------------|----------------|
| SISOKR | 0.4% | 2.8% | 0.015 |
| SciBERT Regression | 16.8% | 56.9% | 0.298 |
| CMAM - MLP | 34.9% | 84.2% | 0.513 |
| CMAM - GCN | 33.2% | 82.5% | 0.495 |
| CMAM - Ensemble (MLP \times 3) | 39.8% | 87.6% | 0.562 |
| CMAM - Ensemble (GCN \times 3) | 39.0% | 87.0% | 0.551 |
| CMAM - Ensemble (MLP \times 3 + GCN \times 3) | 44.2% | 88.7% | 0.597 |
| DSOKR - SubSample Sketch | 48.2% | 87.4% | 0.624 |
| DSOKR - Gaussian Sketch | 49.0% | 87.5% | 0.630 |
| DSOKR - Ensemble (SubSample \times 3) | 51.0% | 88.2% | 0.642 |
| DSOKR - Ensemble (Gaussian \times 3) | 50.5% | 87.9% | 0.642 |
| DSOKR - Ensemble (SubSample \times 3 + Gaussian \times 3) | 50.0% | 88.3% | 0.640 |

kernels: Cosine kernel and Gaussian kernel with gamma chosen from $\{10^{-9}, 10^{-6}, 10^{-3}, 1\}$, along with the following three sketches: sub-sampling (Rudi et al., 2015), Gaussian (Yang et al., 2017), and p -sparsified (El Ahmad et al., 2023). The sketching size for all combinations of the output kernels and sketches is determined using the *Perfect h* strategy. As for the baselines, we consider SciBERT Regression, Cross-Modal Attention Model (CMAM) (Edwards et al., 2021), and SISOKR. In the case of SciBERT Regression, we address the regression problem using Mean Squared Error loss, where the output space is the embedding space of Mol2vec, within a function space parameterized by SciBERT. CMAM aims to enhance the cosine similarity between the text embedding and the corresponding molecule in true pairs by employing a contrastive loss function. Specifically, the former is derived from SciBERT, while the latter is generated using either a multi-layer perceptron (MLP) or a graph convolutional network (GCN) atop the Mol2vec representation. We reproduce the results of CMAM with the codes² released by Edwards et al. (2021). In SISOKR, we use SciBERT embeddings as input features, leveraging the cosine kernel atop them. We maintain the identical output kernel sketching setup as in DSOKR. For all methods, we train the model using the best hyper-parameters with three random seeds and report the one with the best validation performance. The performance is evaluated with mean reciprocal rank (MRR), Hits@1 and Hits@10. We could not benchmark AMAN (Zhao et al., 2024), as no implementation is publicly available.

²<https://github.com/cnedwards/text2mol>

Ensemble. In Edwards et al. (2021), the authors propose an ensemble strategy to enhance the results by aggregating the ranks obtained by different training of their models. If for each $1 \leq t \leq T$, R_t denotes the ranking returned by the model t , the new score is computed as follows

$$s(y_i) = \sum_{t=1}^T w_t R_t(y_i) \quad s.t. \quad \sum_{i=1}^T \omega_t = 1 \quad (14)$$

for each y_i in the candidate set. In our case, the computation of DSOKR’s last layer g_E depends on a draw of the sketching matrix R , which means that DSOKR is particularly well-suited to the aggregation via multiple draws of the sketching matrix R_t and the training of the corresponding neural networks g_{W_t} . Hence, we explore two more ways of aggregating multiple DSOKR models, by averaging or maximizing these models’ scores, i.e. for any input x and candidate y ,

$$s(x, y) = \sum_{t=1}^T \omega_t g_{W_t}(x)^\top \tilde{\psi}_t(y) \quad \text{or} \quad s(x, y) = \arg \max_{1 \leq t \leq T} g_{W_t}(x)^\top \tilde{\psi}_t(y). \quad (15)$$

We explore all three ensemble methods for DSOKR models and subsequently select the optimal one based on its validation performance.

Experimental results. Figure 5 illustrates the validation MRR scores with *Perfect h*, for many m values, and either Cosine or Gaussian output kernels. It is evident that for both the Cosine kernel and Gaussian kernel (with $\gamma = 10^{-6}$) employing various sketching methods, the MRR score stabilizes as the sketching size exceeds 100, and that Cosine outperforms Gaussian. This observation allows us to choose $m = 100$, smaller than the original Mol2vec dimension, which is 300. Table 2 presents a comprehensive comparison of DSOKR with various baseline models. Firstly, comparing DSOKR with SISOKR reveals the critical importance of employing deep neural networks when dealing with complex structured inputs and DSOKR makes it possible in the case of functional output space. Secondly, the notable improvement over SciBERT Regression underscores the value of employing kernel sketching to derive more compact and better output features, thereby facilitating regression problem-solving. Lastly, DSOKR outperforms the sota CMAP for both single and ensemble models. See Appendix C.2 for more details.

4 Conclusion

We designed a new architecture of neural networks able to minimize kernel-induced losses for structured prediction and achieving sota performance on molecular identification. An interesting avenue for future work is to derive excess risk for this estimator by combining deep learning theory and surrogate regression bounds.

Acknowledgments and Disclosure of Funding

Funded by the European Union. Views and opinions expressed are however those of the author(s) only and do not necessarily reflect those of the European Union or European Commission. Neither the European Union nor the granting authority can be held responsible for them. This project has received funding from the European Union’s Horizon Europe research and innovation programme under grant agreement 101120237 (ELIAS), the Télécom Paris research chair on Data Science and Artificial Intelligence for Digitalized Industry and Services (DSADIS) and the PEPR-IA through the project FOUNDRY.

References

- Alaoui, A. and Mahoney, M. W. (2015). Fast randomized kernel ridge regression with statistical guarantees. In Cortes, C., Lawrence, N., Lee, D., Sugiyama, M., and Garnett, R., editors, *Advances in Neural Information Processing Systems (NeurIPS)*, volume 28.
- Bach, F. (2013). Sharp analysis of low-rank kernel matrix approximations. In *Proc. of the 26th annual Conference on Learning Theory*, pages 185–209. PMLR.

- Bakir, G., Hofmann, T., Smola, A. J., Schölkopf, B., and Taskar, B. (2007). *Predicting structured data*. The MIT Press.
- Belanger, D. and McCallum, A. (2016). Structured prediction energy networks. In *International Conference on Machine Learning*, pages 983–992.
- Belanger, D., Yang, B., and McCallum, A. (2017). End-to-end learning for structured prediction energy networks. In Precup, D. and Teh, Y. W., editors, *Proceedings of the 34th International Conference on Machine Learning*, volume 70 of *Proceedings of Machine Learning Research*, pages 429–439. PMLR.
- Beltagy, I., Lo, K., and Cohan, A. (2019). SciBERT: A Pretrained Language Model for Scientific Text. In Inui, K., Jiang, J., Ng, V., and Wan, X., editors, *Proceedings of the 2019 Conference on Empirical Methods in Natural Language Processing and the 9th International Joint Conference on Natural Language Processing (EMNLP-IJCNLP)*, pages 3615–3620, Hong Kong, China. Association for Computational Linguistics.
- Borgwardt, K., Ghisu, E., Llinares-López, F., O’Bray, L., and Rieck, B. (2020). Graph kernels: State-of-the-art and future challenges. *Foundations and Trends in Machine Learning*, 13(5-6):531–712.
- Borgwardt, K. and Kriegel, H. (2005). Shortest-path kernels on graphs. In *Fifth IEEE International Conference on Data Mining (ICDM’05)*, pages 8 pp.-.
- Brogat-Motte, L., Flamary, R., Brouard, C., Rousu, J., and D’Alché-Buc, F. (2022). Learning to Predict Graphs with Fused Gromov-Wasserstein Barycenters. In Chaudhuri, K., Jegelka, S., Song, L., Szepesvari, C., Niu, G., and Sabato, S., editors, *Proceedings of the 39th International Conference on Machine Learning*, volume 162 of *Proceedings of Machine Learning Research*, pages 2321–2335. PMLR.
- Brouard, C., d’Alché-Buc, F., and Szafranski, M. (2011). Semi-supervised penalized output kernel regression for link prediction. In *International Conference on Machine Learning (ICML)*, pages 593–600.
- Brouard, C., Shen, H., Dührkop, K., d’Alché-Buc, F., Böcker, S., and Rousu, J. (2016a). Fast metabolite identification with input output kernel regression. *Bioinformatics*, 32(12):28–36.
- Brouard, C., Szafranski, M., and D’Alché-Buc, F. (2016b). Input output kernel regression: supervised and semi-supervised structured output prediction with operator-valued kernels. *The Journal of Machine Learning Research*, 17(1):6105–6152.
- Cabannes, V. A., Bach, F., and Rudi, A. (2021). Fast rates for structured prediction. In *conference on learning theory*, pages 823–865. PMLR.
- Ciliberto, C., Rosasco, L., and Rudi, A. (2016). A consistent regularization approach for structured prediction. In *Advances in Neural Information Processing Systems (NIPS) 29*, pages 4412–4420.
- Ciliberto, C., Rosasco, L., and Rudi, A. (2020). A general framework for consistent structured prediction with implicit loss embeddings. *J. Mach. Learn. Res.*, 21(98):1–67.
- Cortes, C., Mohri, M., and Weston, J. (2005). A general regression technique for learning transductions. In *International Conference on Machine Learning (ICML)*, pages 153–160.
- Cortes, C., Mohri, M., and Weston, J. (2007). A general regression framework for learning string-to-string mappings. In *Predicting Structured Data*.
- Costa, F. and Grave, K. D. (2010). Fast Neighborhood Subgraph Pairwise Distance Kernel. In *Proceedings of the 27th International Conference on International Conference on Machine Learning, ICML’10*, pages 255–262, Madison, WI, USA. Omnipress. event-place: Haifa, Israel.
- Deshwal, A., Doppa, J. R., and Roth, D. (2019). Learning and inference for structured prediction: A unifying perspective. In *Proceedings of the Twenty-Eighth International Joint Conference on Artificial Intelligence (IJCAI-19)*.
- Drineas, P., Mahoney, M. W., and Cristianini, N. (2005). On the nystrom method for approximating a gram matrix for improved kernel-based learning. *JMLR*, 6(12).

- Edwards, C., Zhai, C., and Ji, H. (2021). Text2Mol: Cross-Modal Molecule Retrieval with Natural Language Queries. In Moens, M.-F., Huang, X., Specia, L., and Yih, S. W.-t., editors, *Proceedings of the 2021 Conference on Empirical Methods in Natural Language Processing*, pages 595–607, Online and Punta Cana, Dominican Republic. Association for Computational Linguistics.
- El Ahmad, T., Brogat-Motte, L., Laforgue, P., and d’Alché Buc, F. (2024). Sketch in, sketch out: Accelerating both learning and inference for structured prediction with kernels. In Dasgupta, S., Mandt, S., and Li, Y., editors, *Proceedings of The 27th International Conference on Artificial Intelligence and Statistics*, volume 238 of *Proceedings of Machine Learning Research*, pages 109–117. PMLR.
- El Ahmad, T., Laforgue, P., and d’Alché Buc, F. (2023). Fast kernel methods for generic lipschitz losses via p -sparsified sketches. *Transactions on Machine Learning Research*.
- Gärtner, T. (2008). *Kernels for Structured Data*, volume 72 of *Series in Machine Perception and Artificial Intelligence*. WorldScientific.
- Geurts, P., Wehenkel, L., and d’Alché Buc, F. (2006). Kernelizing the output of tree-based methods. In *Proceedings of the 23rd International Conference on Machine Learning, ICML ’06*, page 345–352, New York, NY, USA. Association for Computing Machinery.
- Graber, C., Meshi, O., and Schwing, A. (2018). Deep structured prediction with nonlinear output transformations. *Advances in Neural Information Processing Systems*, 31.
- Gygli, M., Norouzi, M., and Angelova, A. (2017). Deep value networks learn to evaluate and iteratively refine structured outputs. In *Proceedings of the 34th International Conference on Machine Learning - Volume 70, ICML’17*, page 1341–1351. JMLR.org.
- Hagberg, A. A., Schult, D. A., and Swart, P. J. (2008). Exploring Network Structure, Dynamics, and Function using NetworkX. In Varoquaux, G., Vaught, T., and Millman, J., editors, *Proceedings of the 7th Python in Science Conference*, pages 11 – 15, Pasadena, CA USA.
- Hastings, J., Owen, G., Dekker, A., Ennis, M., Kale, N., Muthukrishnan, V., Turner, S., Swainston, N., Mendes, P., and Steinbeck, C. (2016). ChEBI in 2016: Improved services and an expanding collection of metabolites. *Nucleic Acids Research*, 44(D1):D1214–D1219.
- Huber, P. J. (1964). Robust estimation of a location parameter. *The Annals of Mathematical Statistics*, pages 73–101.
- Jaeger, S., Fulle, S., and Turk, S. (2018). Mol2vec: Unsupervised Machine Learning Approach with Chemical Intuition. *Journal of Chemical Information and Modeling*, 58(1):27–35.
- Jumper, J., Evans, R., Pritzel, A., Green, T., Figurnov, M., Ronneberger, O., Tunyasuvunakool, K., Bates, R., Žídek, A., Potapenko, A., et al. (2021). Highly accurate protein structure prediction with alphafold. *Nature*, 596(7873):583–589.
- Kadri, H., Ghavamzadeh, M., and Preux, P. (2013). A generalized kernel approach to structured output learning. In *International Conference on Machine Learning (ICML)*, pages 471–479.
- Kim, S., Chen, J., Cheng, T., Gindulyte, A., He, J., He, S., Li, Q., Shoemaker, B. A., Thiessen, P. A., Yu, B., Zaslavsky, L., Zhang, J., and Bolton, E. E. (2019). PubChem 2019 update: improved access to chemical data. *Nucleic Acids Research*, 47(D1):D1102–D1109.
- Kim, S., Thiessen, P. A., Bolton, E. E., Chen, J., Fu, G., Gindulyte, A., Han, L., He, J., He, S., Shoemaker, B. A., Wang, J., Yu, B., Zhang, J., and Bryant, S. H. (2016). PubChem Substance and Compound databases. *Nucleic Acids Research*, 44(D1):D1202–D1213.
- Kingma, D. P. and Ba, J. (2015). Adam: A method for stochastic optimization. In Bengio, Y. and LeCun, Y., editors, *3rd International Conference on Learning Representations, ICLR 2015, San Diego, CA, USA, May 7-9, 2015, Conference Track Proceedings*.
- Kirillov, A., Mintun, E., Ravi, N., Mao, H., Rolland, C., Gustafson, L., Xiao, T., Whitehead, S., Berg, A. C., Lo, W.-Y., et al. (2023). Segment anything. In *Proceedings of the IEEE/CVF International Conference on Computer Vision*, pages 4015–4026.

- Korba, A., Garcia, A., and d'Alché-Buc, F. (2018). A structured prediction approach for label ranking. In Bengio, S., Wallach, H., Larochelle, H., Grauman, K., Cesa-Bianchi, N., and Garnett, R., editors, *Advances in Neural Information Processing Systems*, volume 31. Curran Associates, Inc.
- Kpotufe, S. and Sriperumbudur, B. K. (2020). Gaussian sketching yields a J-L lemma in RKHS. In Chiappa, S. and Calandra, R., editors, *AISTATS 2020*, volume 108 of *Proceedings of Machine Learning Research*, pages 3928–3937. PMLR.
- Lacotte, J. and Pilanci, M. (2022). Adaptive and oblivious randomized subspace methods for high-dimensional optimization: Sharp analysis and lower bounds. *IEEE Transactions on Information Theory*, 68(5):3281–3303.
- Laforgue, P., Lambert, A., Brogat-Motte, L., and d'Alché Buc, F. (2020). Duality in rkhs with infinite dimensional outputs: Application to robust losses. In *International Conference on Machine Learning*, pages 5598–5607. PMLR.
- LeCun, Y., Chopra, S., Hadsell, R., Ranzato, A., and Huang, F. J. (2006). A tutorial on energy-based learning. In *Predicting structured data*.
- Lee, J.-Y., Patel, D., Goyal, P., Zhao, W., Xu, Z., and McCallum, A. (2022). Structured energy network as a loss. In Oh, A. H., Agarwal, A., Belgrave, D., and Cho, K., editors, *Advances in Neural Information Processing Systems*.
- Li, Z., Ton, J.-F., Oglic, D., and Sejdinovic, D. (2021). Towards a unified analysis of random fourier features. *Journal of Machine Learning Research*, 22(108):1–51.
- Mahoney, M. W. et al. (2011). Randomized algorithms for matrices and data. *Foundations and Trends® in Machine Learning*, 3(2):123–224.
- Meanti, G., Carratino, L., Rosasco, L., and Rudi, A. (2020). Kernel methods through the roof: Handling billions of points efficiently. *Advances in Neural Information Processing Systems (NeurIPS)*, 33.
- Meanti, G., Chatalic, A., Kostic, V. R., Novelli, P., massimiliano pontil, and Rosasco, L. (2023). Estimating koopman operators with sketching to provably learn large scale dynamical systems. In *Thirty-seventh Conference on Neural Information Processing Systems*.
- Nikolentzos, G., Meladianos, P., Limnios, S., and Vazirgiannis, M. (2018). A Degeneracy Framework for Graph Similarity. In *Proceedings of the Twenty-Seventh International Joint Conference on Artificial Intelligence, IJCAI-18*, pages 2595–2601. International Joint Conferences on Artificial Intelligence Organization.
- Nowak, A., Bach, F., and Rudi, A. (2019). Sharp analysis of learning with discrete losses. In Chaudhuri, K. and Sugiyama, M., editors, *Proceedings of the Twenty-Second International Conference on Artificial Intelligence and Statistics (AISTATS)*, volume 89 of *Proceedings of Machine Learning Research*, pages 1920–1929.
- Nowak, A., Bach, F., and Rudi, A. (2020). Consistent structured prediction with max-min margin Markov networks. In III, H. D. and Singh, A., editors, *Proceedings of the 37th International Conference on Machine Learning*, volume 119 of *Proceedings of Machine Learning Research*, pages 7381–7391. PMLR.
- Nowozin, S. and Lampert, C. H. (2011). Structured learning and prediction in computer vision. *Foundations and Trends in Computer Graphics and Vision*, 6(3-4):185–365.
- Rahimi, A. and Recht, B. (2007). Random features for large scale kernel machines. *NIPS*, 20:1177–1184.
- Ralaivola, L., Swamidass, S. J., Saigo, H., and Baldi, P. (2005). Graph kernels for chemical informatics. *Neural Networks*, 18(8):1093–1110. Neural Networks and Kernel Methods for Structured Domains.
- Ramakrishnan, R., Dral, P. O., Rupp, M., and von Lilienfeld, O. A. (2014). Quantum chemistry structures and properties of 134 kilo molecules. *Scientific Data*, 1. Publisher: Nature Publishing Group.

- Ruddigkeit, L., van Deursen, R., Blum, L. C., and Reymond, J.-L. (2012). Enumeration of 166 Billion Organic Small Molecules in the Chemical Universe Database GDB-17. *Journal of Chemical Information and Modeling*, 52(11):2864–2875. Publisher: American Chemical Society.
- Rudi, A., Camoriano, R., and Rosasco, L. (2015). Less is more: Nyström computational regularization. *Advances in Neural Information Processing Systems*, 28.
- Rudi, A. and Rosasco, L. (2017). Generalization properties of learning with random features. In *Advances on Neural Information Processing Systems (NeurIPS)*, pages 3215–3225.
- Schölkopf, B., Smola, A., and Müller, K.-R. (1997). Kernel principal component analysis. In *International conference on Artificial Neural Networks (ICANN)*, pages 583–588. Springer.
- Seidman, S. B. (1983). Network structure and minimum degree. *Social Networks*, 5(3):269–287.
- Shervashidze, N., Schweitzer, P., van Leeuwen, E. J., Mehlhorn, K., and Borgwardt, K. M. (2011). Weisfeiler-lehman graph kernels. *Journal of Machine Learning Research*, 12(77):2539–2561.
- Siglidis, G., Nikolentzos, G., Limnios, S., Giatsidis, C., Skianis, K., and Vazirgiannis, M. (2020). Grakel: A graph kernel library in python. *Journal of Machine Learning Research*, 21(54):1–5.
- Steinwart, I. and Christmann, A. (2008). Sparsity of svms that use the epsilon-insensitive loss. In Koller, D., Schuurmans, D., Bengio, Y., and Bottou, L., editors, *Advances in Neural Information Processing Systems 21 (NeurIPS)*, pages 1569–1576. Curran Associates, Inc.
- Serge, N., Sriperumbudur, B., Rosasco, L., and Rudi, A. (2020). Gain with no pain: Efficiency of kernel-pca by nyström sampling. In Chiappa, S. and Calandra, R., editors, *Proceedings of the Twenty Third International Conference on Artificial Intelligence and Statistics*, volume 108 of *Proceedings of Machine Learning Research*, pages 3642–3652. PMLR.
- Serge, N. and Sriperumbudur, B. K. (2022). Statistical optimality and computational efficiency of nystrom kernel pca. *Journal of Machine Learning Research*, 23(337):1–32.
- Tanimoto, T. (1958). *An Elementary Mathematical Theory of Classification and Prediction*. International Business Machines Corporation.
- Tripp, A., Bacallado, S., Singh, S., and Hernández-Lobato, J. M. (2023). Tanimoto random features for scalable molecular machine learning. In *Thirty-seventh Conference on Neural Information Processing Systems*.
- Tu, L. and Gimpel, K. (2018). Learning approximate inference networks for structured prediction. In *International Conference on Learning Representations*.
- Vaswani, A., Shazeer, N., Parmar, N., Uszkoreit, J., Jones, L., Gomez, A. N., Kaiser, L., and Polosukhin, I. (2017). Attention is All you Need. In *Advances in Neural Information Processing Systems (NIPS)*, pages 5998–6008.
- Vayer, T., Courty, N., Tavenard, R., Laetitia, C., and Flamary, R. (2019). Optimal Transport for structured data with application on graphs. In Chaudhuri, K. and Salakhutdinov, R., editors, *Proceedings of the 36th International Conference on Machine Learning*, volume 97 of *Proceedings of Machine Learning Research*, pages 6275–6284. PMLR.
- Weisfeiler, B. and Leman, A. (1968). The reduction of a graph to canonical form and the algebra which appears therein. *nti, Series*, 2(9):12–16.
- Weston, J., Chapelle, O., Vapnik, V., Elisseeff, A., and Schölkopf, B. (2003). Kernel dependency estimation. In Becker, S., Thrun, S., and Obermayer, K., editors, *Advances in Neural Information Processing Systems 15*, pages 897–904. MIT Press.
- Williams, C. and Seeger, M. (2001). Using the nyström method to speed up kernel machines. In Leen, T., Dietterich, T., and Tresp, V., editors, *Advances in Neural Information Processing Systems*, volume 13, pages 682–688. MIT Press.
- Woodruff, D. P. (2014). Sketching as a tool for numerical linear algebra. *Found. Trends Theor. Comput. Sci.*, 10(1-2):1–157.

- Yang, T., Li, Y.-f., Mahdavi, M., Jin, R., and Zhou, Z.-H. (2012). Nyström method vs random fourier features: A theoretical and empirical comparison. In Pereira, F., Burges, C. J. C., Bottou, L., and Weinberger, K. Q., editors, *Advances in Neural Information Processing Systems*, volume 25. Curran Associates, Inc.
- Yang, Y., Pilanci, M., Wainwright, M. J., et al. (2017). Randomized sketches for kernels: Fast and optimal nonparametric regression. *The Annals of Statistics*, 45(3):991–1023.
- Zhao, W., Zhou, D., Cao, B., Zhang, K., and Chen, J. (2024). Adversarial Modality Alignment Network for Cross-Modal Molecule Retrieval. *IEEE Transactions on Artificial Intelligence*, 5(1):278–289.

A Technical proof

We here provide the proof of Proposition 2.

Proposition 2. Given the pre-trained basis $\tilde{E} = (\tilde{e}_j)_{j \leq p}$, $L(\tilde{E}, W)$ expresses as

$$L(\tilde{E}, W) = \frac{1}{n} \sum_{i=1}^n \left\| g_W(x_i) - \tilde{\psi}(y_i) \right\|_2^2, \quad (8)$$

where $\tilde{\psi}(y) = (\tilde{e}_1(y), \dots, \tilde{e}_p(y))^\top = \tilde{D}_p^{-1/2} \tilde{V}_p^\top \mathbf{R} \mathbf{k}^y \in \mathbb{R}^p$, $\tilde{V}_p = (\tilde{\mathbf{v}}_1, \dots, \tilde{\mathbf{v}}_p)$, $\tilde{D}_p = \text{diag}(\sigma_1(\tilde{\mathbf{K}}), \dots, \sigma_p(\tilde{\mathbf{K}}))$, and $\mathbf{k}^y = (\mathbf{k}(y, y_1), \dots, \mathbf{k}(y, y_n))$.

Proof. For any pair $(x, y) \in \mathcal{X} \times \mathcal{Y}$, the loss function is given by

$$\begin{aligned} \|h_\theta(x) - \psi(y)\|_{\mathcal{H}}^2 &= \left\| \sum_{i=1}^p g_W(x)_i \tilde{e}_i - \psi(y) \right\|_{\mathcal{H}}^2 \\ &= \sum_{i,j=1}^p g_W(x)_i g_W(x)_j \langle \tilde{e}_i, \tilde{e}_j \rangle_{\mathcal{H}} - 2 \sum_{j=1}^p g_W(x)_j \langle \tilde{e}_j, \psi(y) \rangle_{\mathcal{H}} + k(y, y) \\ &= \|g_W(x)\|_2^2 - 2g_W(x)^\top \tilde{\psi}(y) + k(y, y), \end{aligned}$$

since \tilde{E} is an orthonormal basis, and $\langle \tilde{e}_j, \psi(y) \rangle_{\mathcal{H}} = \tilde{e}_j(y) = \tilde{\psi}(y)_j$ by the reproducing property. Noting that

$$\left\| g_W(x) - \tilde{\psi}(y) \right\|_2^2 = \|g_W(x)\|_2^2 - 2g_W(x)^\top \tilde{\psi}(y) + \left\| \tilde{\psi}(y) \right\|_2^2, \quad (16)$$

and that both $k(y, y)$ and $\left\| \tilde{\psi}(y) \right\|_2^2$ are independent of W concludes the proof. \square

B Graph Prediction via Output Kernel Regression

In this section, we present kernel examples to tackle graph prediction via Output Kernel Regression.

A graph G is defined by its sets of vertices V and edges E . Besides, it may contain either node labels or attributes, or edge labels, attributes, or weights. Before giving some examples of kernels dealing directly with graphs, we present examples of kernels dealing with fingerprints.

Fingerprints. Indeed, when manipulating molecules, either for molecular property prediction or molecule identification, many works use fingerprints to represent graphs (Ralaivola et al., 2005; Brouard et al., 2016a,b; Tripp et al., 2023). A fingerprint is a binary vector of length $d \geq 1$ and each entry of the fingerprint encodes the presence or absence of a substructure within the graph based on a dictionary. Hence, when using fingerprints, the problem of graph prediction becomes a high-dimensional multi-label prediction problem. A very popular kernel to handle fingerprints is the Tanimoto kernel (Tanimoto, 1958), which basically consists of an intercept over union measure between two fingerprints.

Graph kernels. In this work, we also manipulate raw graphs. Many kernels exist to handle graphs, we present a few that we will use during the experiments. For more details about these kernels and other graph kernel examples, see the documentation of the GraKel library (Siglidis et al., 2020).

Definition 1 (Vertex Histogram kernel). Let $G = (V, E)$ and $G' = (V', E')$ be two node-labeled graphs. Let $\mathcal{L} = \{1, \dots, d\}$ be the set of labels, and $\ell : v \in V \mapsto \ell(v) \in \mathcal{L}$ be the function that assigns a label for each vertex. Then, the vertex label histogram of G is a vector $f = (f_1, \dots, f_d)^\top$, such that $f_i = |\{v \in V : \ell(v) = i\}|$ for each $i \in \mathcal{L}$. Let f, f' be the vertex label histograms of G, G' , respectively. The vertex histogram kernel is then defined as the linear kernel between f and f' , that is

$$\mathbf{k}(G, G') = f^\top f'. \quad (17)$$

The VH kernel needs node-labeled graphs and simply compares two graphs based on the number of nodes having each type of label. Its computation is very fast.

Definition 2 (Shortest-Path kernel (Borgwardt and Kriegel, 2005)). Let $G = (V, E)$ and $G' = (V', E')$ be two graphs, and $S = (V, E_S)$ and $S' = (V', E'_{S'})$ their corresponding shortest-path graphs, i.e. the graphs where we only keep the edges contained in the shortest path between every vertex, then $E_S \subseteq E$ and $E'_{S'} \subseteq E'$. The shortest-path kernel is then defined on G and G' as

$$k(G, G') = k(S, S') = \sum_{e \in E} \sum_{e' \in E'} k_{\text{walk}}^{(1)}(e, e'), \quad (18)$$

where $k_{\text{walk}}^{(1)}(e, e')$ is a positive semidefinite kernel on edge walks of length 1.

The SP kernel can handle graphs either without node labels, with node labels, or with node attributes. This information, as well as the shortest path lengths, are encoded into $k_{\text{walk}}^{(1)}$ whose classical choices are Dirac kernels or, more rarely, Brownian bridge kernels. The computation of the SP kernel is very expensive since it takes $\mathcal{O}(n_V)$ time, where n_V denotes the number of nodes.

We present the Neighborhood Subgraph Pairwise Distance kernel (Costa and Grave, 2010). This kernel extracts pairs of subgraphs from each graph and then compares these pairs.

Definition 3 (Neighborhood Subgraph Pairwise Distance kernel (Costa and Grave, 2010)). Let $G = (V, E)$ and $G' = (V', E')$ be two node-labeled and edge-labeled graphs. For $u, v \in V$, $D(u, v)$ denotes the distance between u and v , i.e. the length of the shortest path between them, for $r \geq 1$, $\{u \in V : D(u, v) \leq r\}$ denotes the neighborhood of radius r of a vertex v , i.e. the set of vertices at a distance less than or equal to r from v , for a subset of vertices $S \subseteq V$, $E(S)$ denotes the set of edges that have both end-points in S , and we can define the subgraph with vertex set S and edge set $E(S)$. N_r^v denotes the subgraph induced by $\{u \in V : D(u, v) \leq r\}$. Let also $R_{r,d}(A_v, B_u, G)$ be a relation between two rooted graphs A_v, B_u and a graph $G = (V, E)$ that is true if and only if both A_v and B_u are in $\{N_r^v : v \in V\}$, where we require A_v, B_u to be isomorphic to some N_r^v to verify the set inclusion, and that $D(u, v) = d$. We denote with $R^{-1}(G)$ the inverse relation that yields all the pairs of rooted graphs A_v, B_u satisfying the above constraints. The neighborhood subgraph pairwise distance kernel is then based on the following kernel

$$k_{r,d}(G, G') = \sum_{A_v, B_u \in R_{r,d}^{-1}(G)} \sum_{A'_{v'}, B'_{u'} \in R_{r,d}^{-1}(G')} \delta(A_v, A'_{v'}) \delta(B_u, B'_{u'}), \quad (19)$$

where δ is 1 if its input subgraphs are isomorphic, and 0 otherwise. This counts the number of identical pairs of neighboring subgraphs of radius r at distance d between two graphs. The NSPD kernel is then defined on G and G' as

$$k(G, G') = \sum_{r=0}^{r^*} \sum_{d=0}^{d^*} \hat{k}_{r,d}(G, G'), \quad (20)$$

where $\hat{k}_{r,d}$ is a normalized version of $k_{r,d}$, and r^* and d^* are hyper-parameters of the kernel.

The NSPD takes into account the edge labels, which can be of particular interest when manipulating molecules. For small values of r^* and d^* , its complexity is in practice linear in the size of the graph.

We now introduce the Weisfeiler-Lehman framework, inspired by the Weisfeiler-Lehman test of graph isomorphism (Weisfeiler and Leman, 1968), that operates on top of existing graph kernels. The Weisfeiler-Lehman algorithm replaces the label of each vertex with a multiset label consisting of the original label of the vertex and the sorted set of labels of its neighbors. The resulting multiset is then compressed into a new, short label, and this procedure is repeated for h iterations.

Definition 4 (Weisfeiler-Lehman kernel (Shervashidze et al., 2011)). Let $G = (V, E)$ and $G' = (V', E')$ be two node-labeled graphs, endowed with labeling functions $\ell = \ell_0$ and $\ell' = \ell'_0$, respectively. The Weisfeiler-Lehman graph of G at height i is a graph G_i endowed with a labeling function ℓ_i which has emerged after i iterations of the relabeling procedure described previously. Let k_{base} be any kernel for graphs, called the base kernel. The Weisfeiler-Lehman kernel with h iterations is then defined on G and G' as

$$k(G, G') = k_{\text{base}}(G_0, G'_0) + \dots + k_{\text{base}}(G_h, G'_h). \quad (21)$$

A very popular choice is the Weisfeiler-Lehman subtree kernel, which corresponds to choosing the VH kernel as the base kernel. Its time complexity is $\mathcal{O}(hn_E)$, where n_E denotes the number of edges, which is efficient. We call it the WL-VH kernel.

We finally present the Core kernel framework that, similarly to the WL framework, operates on top of existing graph kernels. It builds upon the notion of k -core decomposition, first introduced to study the cohesion of social networks (Seidman, 1983).

Definition 5 (Core kernel (Nikolentzos et al., 2018)). Let $G = (V, E)$ and $G' = (V', E')$ be two graphs. Let $G_{\text{sub}}(S, E(S))$ be the subgraph induced by the subset of vertices $S \subseteq V$ and the set of edges $E(S)$ that have both end-points in S . Let $d_{G_{\text{sub}}}(v)$ be the degree of a vertex $v \in S$, i.e. the number of vertices that are adjacent to v in G_{sub} . The, G_{sub} is a k -core of G , denoted by C_k , if it is a maximal subgraph of G in which all vertices have a degree at least k . Let k_{base} be any kernel for graphs, called the base kernel. The core variant of this kernel is then defined on G and G' as

$$k(G, G') = k_{\text{base}}(C_0, C'_0) + \dots + k_{\text{base}}(C_{\delta_{\min}^*}, C'_{\delta_{\min}^*}), \quad (22)$$

where δ_{\min}^* is the minimum of the degeneracies of the two graphs, and for all $1 \leq i \leq \delta_{\min}^*$, C_i and C'_i are the i -core subgraphs of G and G' .

The time complexity of computing the k -core decomposition of a graph is $\mathcal{O}(n_V + n_E)$. Moreover, the complexity of computing the core variant of a kernel depends on its complexity, and in general, the complexity added by the core variant is not very high.

C Additional Experimental Details

In this section, we report additional experimental details on both SMI2Mol and ChEBI-20 datasets.

C.1 Additional Experimental Details for SMI2Mol

For DSOKR, we optimize the parameters of neural networks using Adam with a learning rate of 10^{-3} over 50 epochs. We adopt early stopping based on the validation set’s edit distance. The number of transformer layers is chosen from $\{3, 6\}$, the model dimension is selected from $\{256, 512\}$, the number of heads is set to 8, the feed-forward network dimension is set to four times the model dimension, and the dropout probability is set to 0.2.

More examples of predictions can be found in Figure 6.

C.2 Additional Experimental Details for ChEBI-20

For DSOKR, we conducted training on SciBERT for 50 epochs using the Adam optimizer with a learning rate of 3×10^{-5} . Additionally, we implemented a learning rate schedule that linearly decreases from the initial rate set by the optimizer to 0, following a warm-up period of 1000 steps where it linearly increases from 0 to the initial rate. We incorporated early stopping based on the MRR score on the validation set as well.

Figure 7 presents the validation MRR with respect to m obtained by *Perfect h* with a Gaussian output kernel and additional values of γ . The best γ is clearly 10^{-6} since all sketching types attain the performance of the non-sketched *Perfect h*. Table 3 presents all the results gathered on ChEBI-20 with the additional Mean Rank metric. DSOKR under-performs in terms of mean rank compared with CMAM while outperforming it in terms of hits@1, attaining around 50%, and being equivalent to the ensemble CMAM methods in terms of hits@10, attaining around 88%, which means that most of the time, the correct molecule is predicted in the top rankings and even at the top position half of the time, but in the 12% left, the correct molecule falls to a high predicted rank.

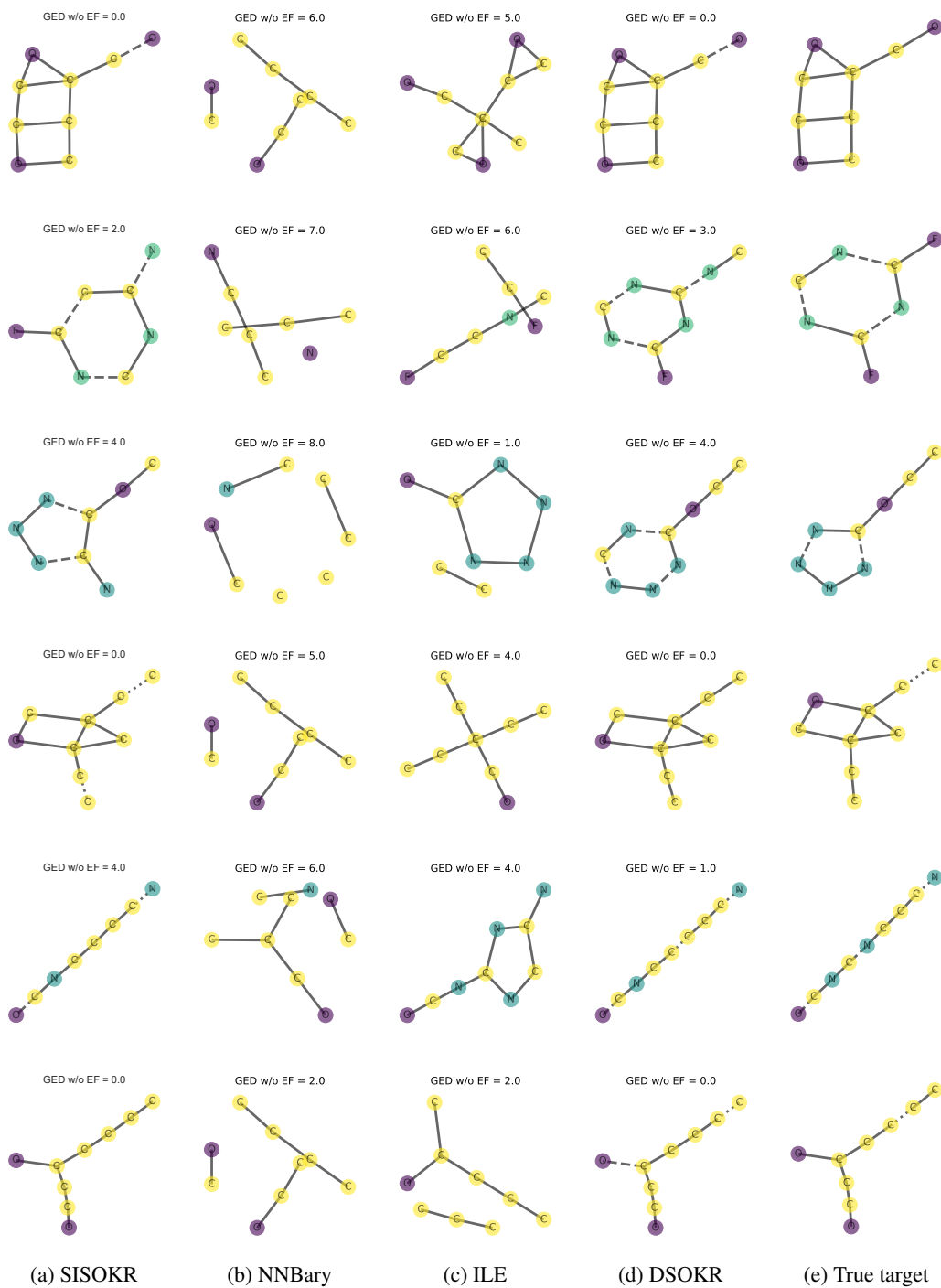


Figure 6: More predicted molecules on the SMI2Mol dataset.

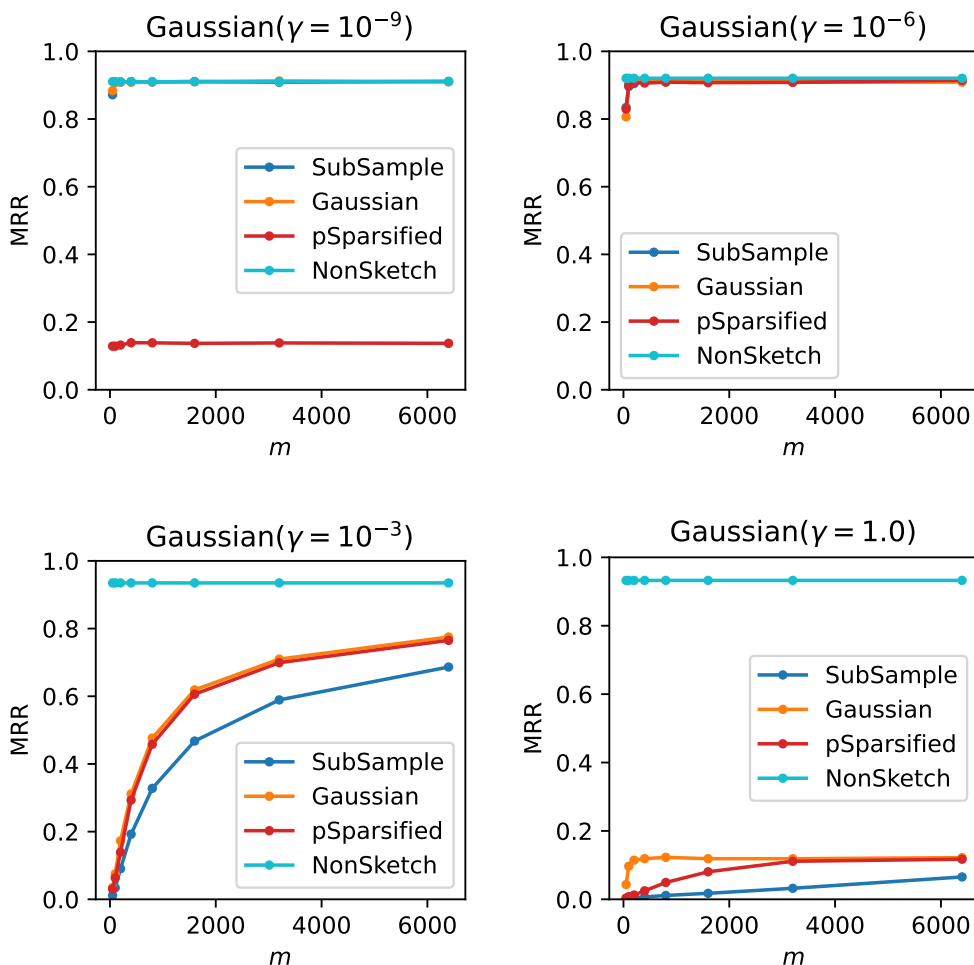


Figure 7: The MRR scores on ChEBI-20 validation set with respect to the sketching size m for *Perfect h* when the output kernel is Gaussian with $\gamma \in \{10^{-9}, 10^{-6}, 10^{-3}, 1.0\}$.

Table 3: Performance of different methods on ChEBI-20 test set. All the methods based on NNs use SciBERT as input text encoder for fair comparison.

| | Mean Rank ↓ | MRR ↑ | Hits@1 ↑ | Hits@10 ↑ |
|-----------------------------------------|--------------|--------------|--------------|--------------|
| SISOKR | 2230.48 | 0.015 | 0.4% | 2.8% |
| SciBERT Regression | 344.53 | 0.298 | 16.8% | 56.9% |
| CMAM - MLP | 23.74 | 0.513 | 34.9% | 84.2% |
| CMAM - GCN | 24.11 | 0.495 | 33.2% | 82.5% |
| CMAM - Ensemble (MLP) | 17.92 | 0.562 | 39.8% | 87.6% |
| CMAM - Ensemble (GCN) | 20.48 | 0.551 | 39.0% | 87.0% |
| CMAM - Ensemble (MLP + GCN) | 16.28 | 0.597 | 44.2% | 88.7% |
| DSOKR - SubSample Sketch | 82.92 | 0.624 | 48.2% | 87.4% |
| DSOKR - Gaussian Sketch | 91.19 | 0.630 | 49.0% | 87.5% |
| DSOKR - Ensemble (SubSample Sketch) | 76.43 | 0.642 | 51.0% | 88.2% |
| DSOKR - Ensemble (Gaussian Sketch) | 81.70 | 0.642 | 50.5% | 87.9% |
| DSOKR - Ensemble (SubSample + Gaussian) | 76.87 | 0.640 | 50.0% | 88.3% |